# Water adsorption on the Be(0001) surface: from monomer to trimer adsorption*

Ning Hua(宁 华), Tao Xiang-Ming(陶向明), and Tan Ming-Qiu(谭明秋)†

*Department of Physics, Zhejiang University, Hangzhou* 310027, *China*

(Received 20 March 2011; revised manuscript received 4 July 2011)

In this paper, the density functional theory has been used to perform a comparative theoretical study of water monomer, dimer, trimer, and bilayer adsorptions on the Be(0001) surface. In our calculations, the adsorbed water molecules are energetically favoured adsorbed on the atop sites, and the dimer adsorption is found to be the most stable with a peak adsorption energy of $\sim$ 437 meV. Further analyses have revealed that the essential bonding interaction between the water monomer and the metal substrate is the hybridization of the water $3a_1$-like molecular orbital with the (s, $p_z$) orbitals of the surface beryllium atoms. While in the case of the water dimer adsorption, the $1b_1$-like orbital of the $H_2O$ molecule plays a dominant role.

**Keywords:** Be(0001)/$H_2O$ surface, adsorption energy, electronic structure

**PACS:** 68.43.Bc, 82.20.Kh, 82.45.Jn **DOI:** 10.1088/1674-1056/21/1/016802

## 1. Introduction

Water is one of the most plentiful and essential compounds existing in nature. During the last few decades, studies of the chemisorption process and the structures of water–metal interfaces have received intensive attention due to their importance for the existence of life and for astrophysics and atmospheric science. Essentially, investigating the interaction of water molecules with metal surfaces is a fundamental subject, which can help to understand more complicated water–metal systems. Generally, water monomers are difficult to detect on a metal surface, even at low temperature. However, many researchers have reported that isolated water monomers, water dimers, and cyclic water hexamers can be adsorbed on the surfaces of Ag(111), Cu(111), Pd(111), Pd(110), *et al.* in experiments.[1–9] The water bilayer formation on noble metals and most of the late 3d, 4d, and 5d transition metals has also been reported by several researchers.[10,11] From a theoretical point of view, a series of adsorptions of water monomers on closely packed metal surfaces, such as Ru(1000),[12] Pt(111),[13,14] Ag(111),[15] Ni/$H_2O$,[16] and Cu(100),[17] have been studied through *ab-initio* investigations.

Though water adsorptions on noble and tradition metal surfaces have been the focus of many investigations, experimental and theoretical studies have seldom been performed on a water–simple metal interface. In fact, the study of water adsorption on simple metal surfaces is also of great importance in fundamental research and applications, as many studies are now being applied to explore the possibility of using simple metals instead of noble and transition metals in some applications. An interesting issue behind this study is whether the water adsorbed on a simple metal has similar properties to that of water–transition (noble) metal systems. The aim of this work is to tackle these and related issues by understanding the interactions and the electronic structures of the water adsorption on the surface of metal beryllium. As a simple metal, the beryllium has a very simple electronic configuration ([He]$2s^2$). It is usually used as a neutron multiplier,[18] and is a very important material in nuclear fusion reactors.[19] In this paper, we perform the first first-principles total-energy calculations for the water adsorption on the Be(0001) surface to understand the essential characteristics of the Be(0001)/$H_2O$ system.

The outline of this paper is as follows. In Section 2, the computational method and the atomic models are described in details. In Section 3, the total-energy calculation results for bulk-phase beryllium, the clean Be(0001) surface, and the free water are presented for calibration and benchmarking purposes; meanwhile,

*Project supported by the National Natural Science Foundation of China (Grant No. 11074217).

†Corresponding author. E-mail: mqtan@zju.edu.cn

© 2012 Chinese Physical Society and IOP Publishing Ltd

water monomer and water cluster adsorptions on the Be(0001) surfaces are shown and discussed. In Section 4, we summarize the essential results and the conclusions obtained in this work.

## 2. Methodology and structural models

In this work, all the calculations are performed using the Vienna *ab-initio* simulation package (VASP)[20,21] with the projector-augmented wave (PAW) approach.[22,23] The generalized gradient approximation (GGA) in the form of Perdew–Burke–Ernzerhof (PBE)[24] is chosen for the exchange–correlation functional. The first-order Methfessel–Paxton method[25] for the Fermi smearing with a width of $\sim 0.2$ eV is used for the Brillouin zone integrations. The Monkhorst–Pack scheme[26] with a $6\times6\times1$ $k$-mesh has been used for the integration of the surface Brillouin zones for $p(3\times3)$ and $(\sqrt{3}\times\sqrt{3})R30^\circ$ supercells. The $p(3\times3)$ for monomer, dimer, and trimer adsorptions and the $(\sqrt{3}\times\sqrt{3})R30^\circ$ for the bilayer adsorption have been used in this work. The energy cut-off for the plane wave expansion has been set to 500 eV. The convergence criteria for the total energy and the Hellmann–Feynman force are taken to be $10^{-5}$ eV and $10^{-2}$ eV/Å, respectively. On the (0001) surface of an hcp crystal, there are four different symmetric adsorption sites in total, known as fcc, hcp, bridge, and atop sites. The adsorption of water on each bonding site on the Be(0001) surface is studied, and the favoured azimuthal orientations of the water molecule on the surface are also considered. The target surface is modeled by a seven-layer Be(0001) slab. We relax the beryllium atoms in the three top-most layers as well as the water and keep the lower four Be(0001) layers fixed to provide an environment for the bulk beryllium substrate. A vacuum region with thickness $\sim$10.0 Å is found to be sufficient to avoid the interference between neighbouring slabs. The water is absorbed on one side of the Be(0001) slab, and the induced dipole moment is taken into account by applying a dipole correction.[27,28] In addition, we address the stability of the Be(0001)/$H_2O$ structures with respect to the adsorption of water by using total-energy calculations and adsorption energy analysis. The adsorption energy of water is defined as

$$E_{\rm ads} = \frac{1}{N}(E_{\rm Be(0001)/water} - NE_{\rm water} - E_{\rm Be(0001)}), \quad (1)$$

where $N$ is the number of water molecules in a surface unit, and $E_{\rm water}$ is the total energy of an isolated water molecule, $E_{\rm Be(0001)}$ and $E_{\rm Be(0001)/water}$ are the total energies of the clean Be(0001) surface and the Be(0001)/ $H_2O$ adsorbate-substrate system, respectively.

## 3. Results and discussion

### 3.1. Bulk and surface properties of beryllium combined with molecular water

In practice, bulk beryllium is nearly a semiconductor, whereas the bonding on the Be(0001) surface is more metallic. In order to understand the properties of bulk beryllium and the Be(0001) surface, a comparison of DFT converged lattice parameters with the experimental values for beryllium will be shown in the following. For hexagonal closely packed bulk beryllium, the optimized lattice constant $a$ and $c/a$ ratio are determined to be 2.27 Å and 1.57, respectively, in the PAW-PBE approach. It is no doubt that the present predictions are in good agreement with previous DFT-GGA calculations.[29,30] The corresponding measured parameters for beryllium are listed as $a = 2.285$ Å and $c/a = 1.569$, respectively.[31] The optimized lattice constant $a$ in this work is about 1.7% smaller than the experimental one. Such a small difference implies a well-converged GGA calculation using the PBE exchange–correlation functional. The calculated $c/a$ ratio accords with the experimental result perfectly. In Table 1, the comparison of the calculated surface relaxation of clean Be(0001) with related references and experiments is shown. In the present work, the surface relaxation calculations have been preformed within a seven-layer Be(0001) slab and with a $p(1\times1)$ periodicity. The conclusions could be stated as follows. The interlayer relaxations $d_{ij}$ between layers $i$ and $j$ with respect to the bulk spacing ($d_0 = 1.78$ Å) are expanded, i.e., $\Delta d_{12} = 3.38\%$, $\Delta d_{23} = 1.42\%$, and $\Delta d_{34} = 0.85\%$, for the three top Be(0001) layers. Actually a surface layer expansion $\Delta d_{12} \sim (5.8\pm0.4)\%$ was reported in a low electron energy diffraction (LEED) analysis, which is larger than this calculation (3.38%). Several first-principles calculations have qualitatively confirmed the surface expansion of the Be(0001) surface.

**Table 1.** Comparison of calculated surface relaxation of the Be(0001) surface with related references and experiments. Symbols $\Delta d_{12}$, $\Delta d_{23}$, and $\Delta d_{34}$ represent relative outer layer expansions.

| | $\Delta d_{12}$/% | $\Delta d_{23}$/% | $\Delta d_{34}$/% |
|---|---|---|---|
| GGA | 3.38 | 1.42 | 0.85 |
| LDA[32] | 3.9 | 2.2 | – |
| LDA[33] | 2.7 | 1.2 | 0.6 |
| LDA[34] | 5.9 | 0.9 | 0.0 |
| LDA[35] | 2.9 | 1.1 | 0.4 |
| LDA[30] | 2.1 | – | – |
| GGA[30] | 2.5 | – | – |
| Exp.[31] | 5.8±0.4 | –0.2±0.5 | 0.2±0.5 |

In Table 1, it is easy to find that all these computed results of the surface relaxation are not evidently in agreement with the experimental values. Among these values, $\Delta d_{12}$ (5.9%) obtained in Ref. [34] is the closest to the experimental results, which was obtained based on the many-body effective potential method and the cluster calculation instead of the periodic slab DFT calculation. Actually, the effective potential and cluster method has not been considered as a suitable and precise approach to study the periodic surface problems due to the poor boundary condition treatment incorporated in this method. At present, it is still unclear why the experiments and the theories disagree as much as they do. One possible explanation is that temperature effects are not included in all of the DFT calculations. In view of these facts, we may speculate that DFT-GGA total energy calculations could be used as a powerful tool to study the surface relaxations of the Be(0001) slab, especially at low temperature.

To illustrate the feasibility of the PAW-PBE approach for describing the water and hydrogen bond, the optimized geometries of the free water monomer and the free water dimer are tabulated in Table 2. The bond angles ($\alpha$, $\beta$) of the free water dimer have been depicted in Fig. 1. Our results show that the calculated configurations of the monomer and the dimer are in excellent agreement with the previous experiments.[36,37]

**Table 2.** Calculated geometries of a water molecule and the free water dimer.

| | | Present | Ref. [14] | Exps. [36] and [37] |
|---|---|---|---|---|
| Water | OH bond length/Å | 0.973 | 0.973 | 0.957 |
| | HOH bond angle/(°) | 104.49 | 104.85 | 104.52 |
| Water dimer | OO distance/Å | 2.88 | 2.86 | 2.98 |
| | $\alpha$/(°) | 3.15 | 2.79 | –1±6 |
| | $\beta$/(°) | 123.10 | 126.35 | 123±6 |
| | formation energy/kJ·mol$^{-1}$ | 21 | 24 | 23 |

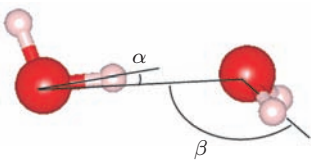



**Fig. 1.** (colour online) Bond angles ($\alpha$, $\beta$) of free water dimer.

## 3.2. Water monomer on Be(0001) surface

The optimized geometries for a monomer on the Be(0001) surface are schematically shown in Fig. 2 and further specified in Table 3. In Table 3, $E_{\rm ads}$ is the adsorption energy, $d_{\rm O-Be}$ stands for the distance of the oxygen atom to the metal surface, $d_{\rm O-H}$ is the bond length of water, $\Delta_{xy}$ is the displacement of the oxygen atom from its precise original site, $\Theta$ is the angle of the water axis away from the surface normal, $\angle$HOH is the HOH bond angle, $\Delta\Phi$ stands for the work function change upon adsorptions, and is defined as $\Delta\Phi = \Phi_{\rm water/slab} - \Phi_{\rm slab}$. For the monomer adsorption, in order to obtain comprehensive research, one isolated water monomer is initially placed on one of the high-symmetry sites, i.e., atop, bridge, fcc, and hcp sites, with various orientations relative to the substrate. Systematically, we also consider the structures of the upright water adsorbed on the above-mentioned high-symmetry sites. All the calculations confirm that the water lies nearly parallel to the Be(0001) surface in every adsorption site (see Table 3 for details). The structural optimization and the total-energy calculation indicate that the atop site is the most stable site compared to the other sites. This observation is further supported by a shorter water–metal (O–Be) bond length (∼1.82 Å) found on the atop site. The favoured azimuthal orientation identified for the monomer on the atop site has one OH bond directed toward an fcc site and the other close to the direction of a bridge site. It is found that the monomer adsorbed on the atop site is laterally displaced from the precise site by 0.11 Å, and the beryllium atom directly beneath the water is slightly displaced along the surface normal from the other top layer atoms.

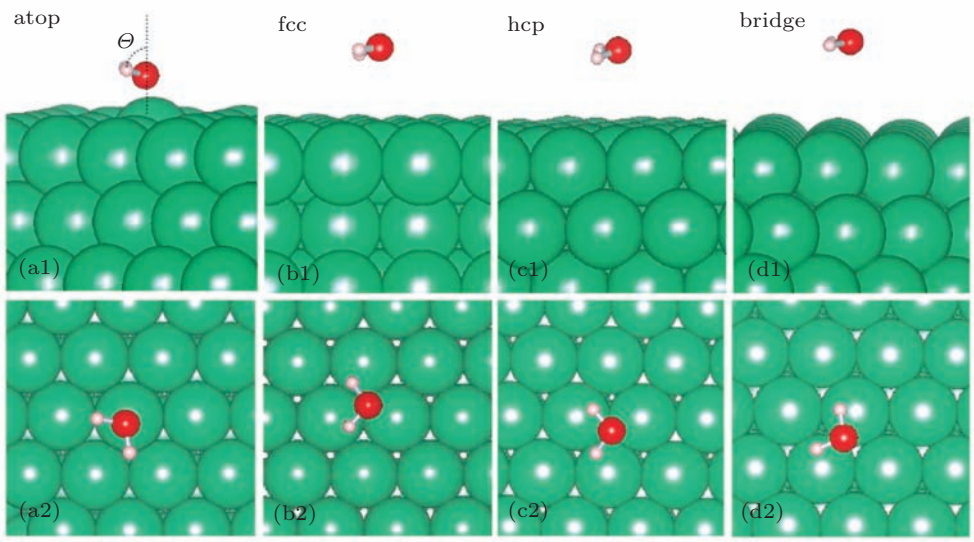



**Fig. 2.** (colour online) Schematic top views (lower panels) and side views (upper panels) of the optimized adsorbed water monomer structures on Be(0001) surface at (a) atop, (b) fcc, (c) hcp, and (d) bridge sites. The related adsorption energies as well as the structural parameters for these configurations are listed in Table 3.

**Table 3.** Adsorption energies and optimized structural parameters for water monomer at high-symmetry sites of Be(0001) surface.

| Site | $E_{\rm ads}$/meV | $d_{\rm O-Be}$/Å | $\Delta_{xy}$/Å | $d_{\rm O-H}$/Å | $\Theta$/(°) | ∠HOH/(°) | $\Delta\Phi$/eV |
|---|---|---|---|---|---|---|---|
| Atop | 271 | 1.82 | 0.11 | 0.98 | 70.0 | 106.10 | –1.60 |
| Bridge | 25 | 3.82 | 0.18 | 0.97 | 88.4 | 104.18 | –0.05 |
| fcc | 26 | 3.39 | 0.11 | 0.97 | 77.6 | 104.11 | 0.19 |
| hcp | 28 | 3.41 | 0.13 | 0.97 | 77.0 | 104.13 | 0.17 |

As shown in Fig. 2(a), the water molecule absorbed on the atop site is tilted approximately 70° away from the surface normal. The OH bond is stretched slightly from the calculated gas-phase value of 0.97 Å to 0.98 Å, and the HOH bond is more open than that in an isolated water molecule. An increased OH bond length and a larger ∠HOH indicate that the electronic charge transfers from the water molecule to the beryllium surface. These results also yield that the water molecules with different axes in respect to the surface normal on the atop site have slightly difference energies. The maximum difference is ∼3 meV, suggesting that the adsorbed water monomer can rotate freely within the two dimensions on the surface. This is in line with previous reports on the water adsorptions on Pd(100), Ru(0001), and Pt(111) surfaces.[12,14,38]

It is unexpected that the higher symmetrical water adsorptions are very unstable due to their reduced adsorption energies (25 meV for bridge, 26 meV for fcc, and 28 meV for hcp). No prominent changes have been found for the bond angles and the bond lengths of the monomer adsorbed on the metastable sites in comparison with those of the water in the gas phase. Actually, the largest difference among the properties of these adsorption sites is the height of the water molecule above the substrate surface (see Fig. 2). The O–Be bond lengths vary from ∼1.82 Å on the atop site to ∼3.5 Å on the fcc site. Considering the relationship between the vertical distance of the oxygen atom from the beryllium substrate and the adsorption energy, Meng *et al.*[14] advanced that a strong adsorption corresponds to a shorter oxygen–metal bond. We have also performed calculations for the surface work function changes upon the water adsorption (see Table 3 for details). A remarkable variation of the surface work function is found in the atop site adsorption case, while such a change is quite small for hcp and the fcc adsorptions. Thus, these results suggest that atop site adsorption with a shorter oxygen–metal bond and a large work function change is favoured on the Be(0001)/$H_2O$ surface.

### 3.3. Water clusters on the Be(0001) surface

The adsorption of water clusters is interesting since both H bonding and water–surface interactions are involved at the same time. Because a water cluster is larger than an isolated water molecule, a larger supercell should be adopted in the periodic calculation of water cluster adsorptions. In this work, a supercell of $p(3\times3)$ is employed for the water dimer and the water trimer, while a smaller slab of $(\sqrt{3}\times\sqrt{3})R30^\circ$ is used for the bilayer adsorption on the Be(0001) surface. The optimized geometries for these structures are depicted in Fig. 3, the energetic and the geometric configurations for each molecule in the clusters are specified in Table 4.

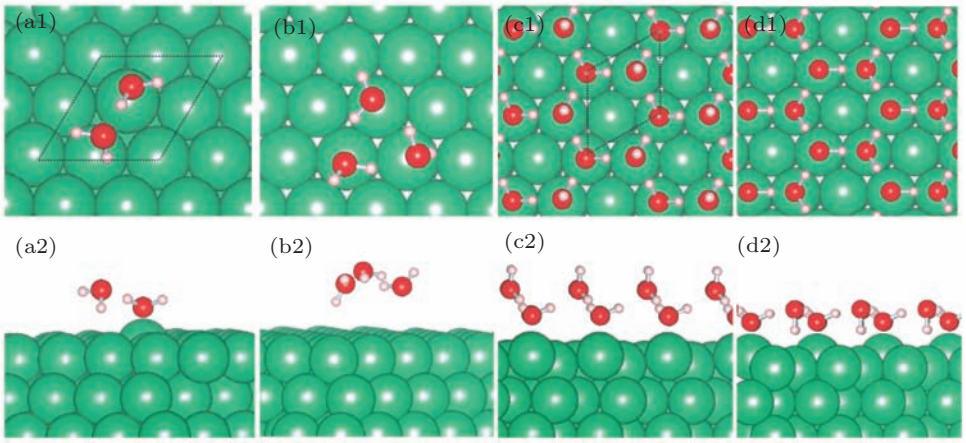



**Fig. 3.** (colour online) Schematic top views (upper panels) and side views (lower panels) of the optimized structures of (a) water dimer, (b) water trimer, (c) H-up bilayer, and (d) H-down bilayer adsorption on Be(0001) surface. The parallelograms in panels (a) and (c) indicate $p(3\times3)$ and $(\sqrt{3}\times\sqrt{3})R30^\circ$ surface unit cells, respectively.

**Table 4.** Structures and energies for water cluster adsorption on Be(0001) surface. Adsorption energies $E_{\rm ads}$, hydrogen bond energies $E_{\rm HB}$, distances, angles, and work-functions are tabulated in units of meV, Å, degree, and eV, respectively.

| Cluster | $E_{\rm ads}$ | $d_{\rm O-Be}$ | $d_{\rm O-H1}$ | $d_{\rm O-H2}$ | $d_{\rm O-O}$ | $\Delta_{xy}$ | $\Theta$ | ∠HOH | $\Phi$ | $E_{\rm HB}$ |
|---|---|---|---|---|---|---|---|---|---|---|
| Monomer | 271 | 1.82 | 0.98 | 0.98 | | 0.11 | 70.0 | 106.10 | 3.79 | |
| Dimer | 437 | 1.72 | 1.02 | 0.98 | 2.62 | 0.02 | 51.8 | 108.37 | 4.11 | 332 |
| | | 3.16 | 0.99 | 0.98 | | 0.14 | 30.6 | 102.27 | | |
| Trimer | 288 | 3.52 | 0.99 | 0.98 | 2.78 | 0.51 | 27.9 | 104.87 | 5.87 | 51 |
| | | 3.34 | 0.99 | 0.97 | 2.78 | 0.18 | 43.9 | 106.10 | | |
| | | 4.14 | 0.99 | 0.97 | 2.81 | 0.33 | 63.8 | 106.48 | | |
| H-up bilayer | 303 | 2.01 | 0.99 | 1.00 | 2.51 | 0.02 | 53.7 | 103.61 | 0.18 | 111 |
| | | 3.74 | 1.05 | 0.97 | | 0.06 | 0.06 | 109.05 | | |
| H-down bilayer | 36 | 1.80 | 1.04 | 1.04 | 2.33 | 0.02 | 48.6 | 102.05 | 3.07 | – |
| | | 3.05 | 1.05 | 1.08 | | 0.02 | 0.06 | 89.10 | | |

For dimer adsorption (see Fig. 3(a)), both water molecules prefer atop sites, forming a configuration similar to that of the free water dimer. The O–O distance in this case ($\sim$2.63 Å) is shorter than that ($\sim$2.88 Å) in the free water dimer case, and the O–H bond in the water molecule is stretched slightly from 0.98 Å to 1.02 Å (see Table 4 for details). We can thus infer that the hydrogen bonding in the adsorbed dimer has been enhanced considerably. The shortest O–Be distances are 1.72 Å and 3.16 Å for the low-lying and the high-lying water molecules, respectively. The two molecules of the adsorbed dimer make an angle of $\beta \sim 102^\circ$, which is smaller than that of a free water dimer. Furthermore, the geometry of the high-lying water molecule is 30.6° away from the surface normal, while the low-lying water molecule lands about 51.8° away. Meanwhile, a narrower ∠HOH and a wider ∠HOH are observed in the high-lying and the low-lying water molecules, respectively. We speculate that these results may be caused by the charge transfer

from the low-lying water molecule into the substrate and the back donation from the beryllium substrate to the high-lying water molecule due to the interaction between the water molecules and the beryllium surface.

As shown in Fig. 3(b), the adsorbed trimer retains its triangle-like shape, and the three water molecules do not lie flat on the surface. In Table 4, an elongated O–H bond and a wider ∠HOH are observed for both the water molecules with the longest and the shortest $d_{\mathrm{O-Be}}$. The lateral displacement $\Delta_{xy}$ of the water molecule in the trimer is larger than those of the molecules in the monomer and the dimer adsorptions.

Finally, the water bilayer adsorption on the Be(0001) surface has been investigated in a similar approach. At higher coverages, water bilayers and water multilayers are considered in the water adsorption. One of the well-known forms is the $(\sqrt{3}\times\sqrt{3})R30^\circ$ bilayer proposed by Doering and Madey, in which the water molecules form a puckered hexagonal network.[39] Such a bilayer structure has been proposed and/or observed on several metal surfaces, including Ru(0001), Pt(111), and Rh(111) surfaces.[12,14,40] In this study, the optimized structural parameters and the adsorption energies of the H-up and the H-down bilayers adsorptions on the Be(0001) surface are presented in Table 4, and the corresponding atomic structures are displayed in Figs. 3(c) and 3(d). As shown in Fig. 3, the configuration of the bilayer in a $(\sqrt{3}\times\sqrt{3})R30^\circ$ surface slab includes two water molecules. Both water molecules are located over the atop sites. The low-lying water molecule lies quite flat on the surface, while the high-lying molecule sits upright in the plane of the surface normal. It is interesting to note that the high-lying water molecule in the H-down case has apparently pressed the low-lying water molecule much closer to the surface, while in the H-up case, the high-lying molecule has pulled the low-lying molecule away from the surface. A wider ∠HOH (H-up) and a narrower ∠HOH (H-down) of the high-lying water molecule of the bilayers are thus observed. The angles ∠HOH of the low-lying molecules in the two cases are smaller than that in the free water molecule case. Meanwhile, the vertical O–O distances have been found to be 1.30 Å and 0.63 Å for the H-up and the H-down bilayers, respectively. The maximum $d_{\mathrm{O-Be}}$ are 3.74 Å and 3.05 Å in the H-up and the H-down bilayer adsorptions, respectively. It is observed that the O–H bonds of the low-lying water molecules in the two bilayer adsorptions tend to be lengthened. The H-bonded O–H distances range approximately from 1.04 Å to 1.07 Å, and the rest of the O–H bond lengths are 0.97 Å and 1.04 Å for the H-up and the H-down bilayer adsorptions, respectively. The difference between the adsorption energies of the H-up and the H-down bilayer structures on Ru(0001), Pt(111), and Rh(111) surfaces is slight.[40] The H-down bilayer structures adsorbed on Pt(111) and Rh(111) surfaces are ∼0.03 eV and 0.02 eV more stable than the corresponding H-up bilayer structures, respectively, whereas, on the Ru(0001) surface, the H-up bilayer structures are more stable. Our calculations suggest that the H-up bilayer adsorption on the Be(0001) surface is energetically favoured and stable, which is similar to the water bilayer adsorption on the Ru(0001) surface, while the H-down bilayer adsorption is so lacking in adsorption energy that the H-down atomic geometry might not be considered as a hopeful candidate in this case.

Among the adsorbed cluster mentioned above, the dimer is the most stable with adsorption energy ∼ 437 meV. The H-down bilayer is the least stable, and the adsorption energy is only ∼36 meV. The H-up bilayer and the trimer lie in between. This energy difference reflects that the H-bonds form dominantly in the adsorbed cluster. In Table 4, we expect that the hydrogen bonding energy in the adsorbed dimer is 332 meV by subtracting the adsorption energy of two monomers (437×2–271×2 meV). This energy is larger than that of the free dimer (∼ 223 meV) calculated in this work, the latter is very close to the experimental value (236±30 meV).[36] The enhancement of the hydrogen bond by the metal substrates can be directly seen from analyzing the valence charge redistribution. On other metal substrates, such as Pd, Rh, Ru, and Au, the water–surface hydrogen bonding enhancement similar to our case has also been observed.[41] For trimer and bilayer adsorptions, the weakened hydrogen bonding is obtained by using the following bond counting method. Here, we use

$$E_{\mathrm{HB}} = (E_{\mathrm{ads}}[\mathrm{bilayer}]\times 2 - E_{\mathrm{ads}}[\mathrm{monomer}])/3, \quad (2)$$

which characterizes the mean H bond formation energy in the bilayer adsorptions. It can be easily seen that the H bond formation energy of the H-up bilayer is one third of that of the dimer case, while the trimer has the minimum energy (∼ 51 meV). The H bond energy of the H-down bilayer adsorption is not listed in Table 4 due to its negative value. In this case, the hydrogen bond is unstable. In reality, the H bonds

and the water–surface bonds for the trimer and the bilayer adsorptions are closely entangled.

## 3.4. Electronic structures

In this section, we turn our attention to the electronic properties of the Be(0001)/$H_2O$ surface. In order to understand the obtained geometrical picture of the water adsorption, we calculate the possible bonding orbitals and the electron density differences to characterize the electronic charge redistribution after the adsorption. The partial densities of states (PDOS) of the water monomer and the water dimer as well as the electron density differences of the monomer, the dimer, and the bilayer adsorbed on the atop site of the Be(0001) surface are computed and discussed.

### 3.4.1. Water monomer adsorption

Firstly, the calculated electronic densities of states (DOS) for the clean and relaxed as well as the water monomer adsorbed Be(0001) surfaces are depicted in Fig. 4. It is obviously seen that the DOS of the surface beryllium atom at the Fermi energy is largely reduced after water adsorption, showing the weaker metallicity of the water-adsorbed Be(0001) surface. The main change of the DOS upon water adsorption is that the highest peak in the plot for the clean Be(0001) surface is decreased and shifted to the energy region below 1.0 eV, meanwhile, two new peaks located respectively at near 7.5 eV and 5.5 eV below the Fermi level are clearly observed.

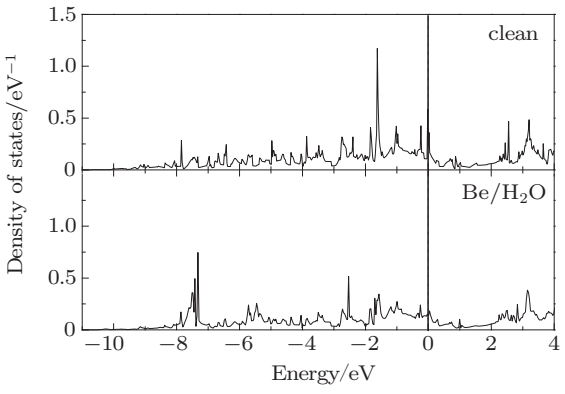



**Fig. 4.** Total densities of states (DOS) for (a) surface beryllium atom of clean Be(0001) surface and (b) beryllium atom beneath the water monomer. The Fermi level is labeled by a dotted line.

In detail, the curve for the PDOS projected onto the oxygen local orbitals for the adsorbed water molecule and the substrate beryllium atom bonded to the water monomer are shown in Fig. 5, where the occupied molecular orbitals of an isolated $H_2O$ are labeled as $1b_2$, $3a_1$, and $1b_1$ respectively. The $2a_1$ orbital of gas-phase water residing at about −22.0 eV is not shown in this figure for simplicity. The PDOS of $H_2O$ projected onto the oxygen local orbitals indicates that the main peaks are contributed by the $1b_2$, $3a_1$, and $1b_1$ orbitals of the $H_2O$ molecule. As the $1b_2$ orbital does not visibly interact with the beryllium surface, to estimate how the other energy levels shift upon adsorption, we have aligned the $1b_2$ level of the gas-phase $H_2O$ to the lowest energy peak of the adsorbed oxygen in Fig. 5(a). Using this energy reference, the PDOS of the oxygen orbitals shows that the $1b_2$-like water molecular orbital is located at ∼10.3 eV below the Fermi level. The first resonance at the $1b_2$-like peak of higher energy is a combination of $p_x$ and $p_y$ states. Upon water adsorption, the $3a_1$-like orbital of the water molecule situated at ∼ 7.5 eV below the Fermi level is observed to shift downward by ∼0.7 eV. Actually, the strongest resonance takes place just at this energy, showing that the $3a_1$-like orbital hybridizes with the beryllium orbitals intensely, which involves s and $p_z$ states. As for the third peak at ∼5.5 eV below the Fermi level, the centre of gravity for energy resides at nearly 0.9 eV below that of the $1b_1$ orbital of an isolated $H_2O$ molecule. The $1b_1$-like orbital has essentially the character of $p_z$ combined with parts of $p_x$ and $p_y$ components, which is wider than the second DOS peak. Therefore, analysis of the PDOS yields that the water monomer is bonded to the Be(0001) surface mainly via the $3a_1$-like orbital and the $3a_1$-like orbital has primarily the characteristics of the oxygen atom.

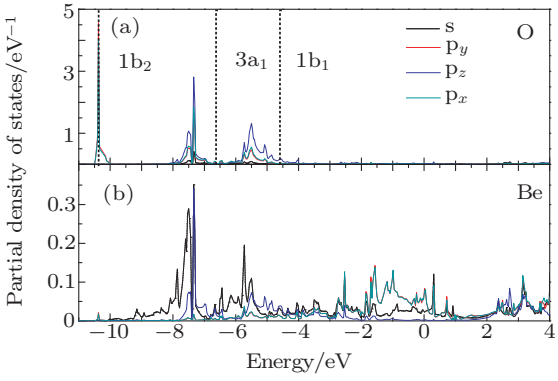



**Fig. 5.** (colour online) (a) Orbital energy diagrams for gas-phase $H_2O$ with the projected PDOS onto the oxygen orbitals for the adsorbed water monomer. (b) The projected PDOS of the beryllium atom bonded to the water molecule. The Fermi level is fixed to zero.

### 3.4.2. Water dimer adsorption

In water dimer adsorption, the PDOS projected onto two oxygen atoms and beryllium atoms bonded to the water molecules are described in Figs. 6 and 7. Similar to the PDOS of the water monomer adsorption on the Be(0001) surface, the $1b_2$ orbital of the gas-phase $H_2O$ has been aligned to the lowest molecule orbital of the oxygen derived for the $H_2O$ dimer. Compared with Fig. 5, we could find some consistent similarities of the PDOS between the water monomer and the bottom water molecule of the dimer adsorption. (i) Both the $p_x$ and the $p_y$ states of oxygen are found to be in the intensity resonances in the first peak, i.e., a clear $1b_2$-like orbital. (ii) Oxygen orbitals involving $p_x$, $p_y$, and $p_z$ are presented in the second peak for the monomer adsorption case, whereas the $p_x$ state has not been observed for the bottom molecule of the dimer adsorption yet.

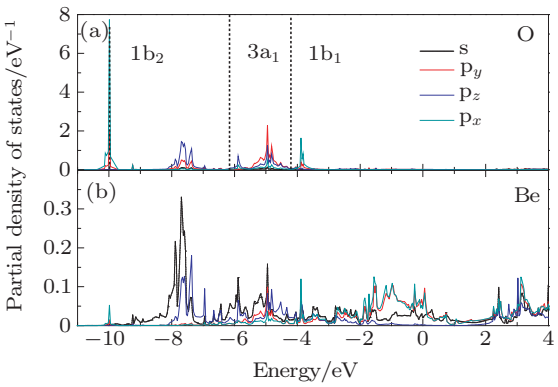



**Fig. 6.** (colour online) (a) Orbital energy diagrams for gas-phase $H_2O$ and the PDOS projected onto the bottom oxygen orbitals for a water dimer adsorbed on the Be(0001) surface. (b) The PDOS projected onto the beryllium atom bonded to water. The Fermi level is set to zero.

(iii) The third peak of the oxygen characteristics is broader than the other states in both cases. Here it is worth pointing out that in Fig. 6 the peak height of the $1b_1$-like orbital is higher than that of the $3a_1$-like orbital, while in the monomer adsorption, the weight of the $3a_1$-like orbital dominates. These results indicate that the $1b_1$-like orbital of the bottom water molecule in the dimer adsorption plays a more important role.

In order to analyze the effects of the bottom water molecule clearly, the PDOS of the top molecule for the water dimer is also calculated and shown in Fig. 7. In this case, the $1b_1$-like and the $3a_1$-like orbitals of the water molecule have only small changes in energy level, i.e., shifting down by $\sim 0.4$ eV in comparison with that of a free water molecule. We conclude that in the dimer adsorption, the bottom water molecule localizes dominantly in the water–surface interaction, while the top one is almost unaffected. Furthermore, the electron density difference for the adsorbed dimer (see Fig. 8(b) for details) also confirms these observations.

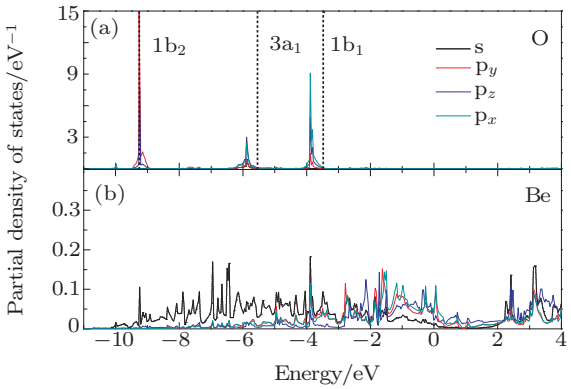



**Fig. 7.** (colour online) (a) Orbital energy diagrams for gas-phase $H_2O$ and the PDOS projected onto the top oxygen orbitals for water dimer adsorbed on the Be(0001) surface. (b) The PDOS projected onto a beryllium atom bonded to water. The Fermi level is set to zero.

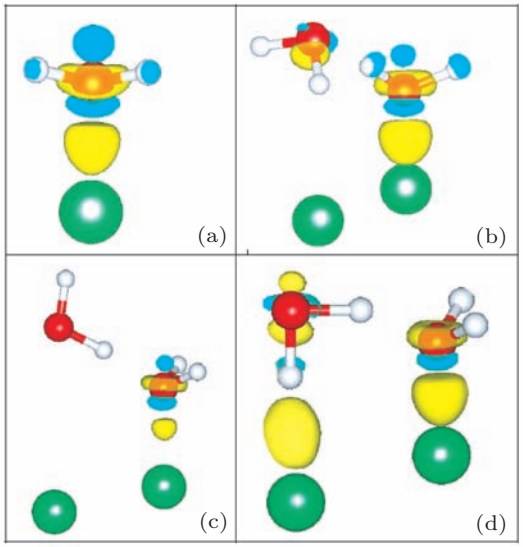



**Fig. 8.** (colour online) Isosurfaces of electron density difference upon adsorption for (a) water monomer, (b) dimer, (c) H-up bilayer, and (d) H-down bilayer adsorptions on Be(0001) surface. Yellow contours indicate an electron density increase, while blue contours indicate an electron density decrease. The isosurface value of the electron density difference is set at $\pm 0.007$ e/Å$^3$.

For examining the electron density difference upon the adsorption and the above orbital based analysis, the electron density difference for the water monomer, the water dimer, the H-up bilayer, and the H-down bilayer adsorptions on the Be(0001) surface are calculated. The electron density difference reveals

the redistribution of charge upon the adsorption. In this work, the electron density difference is defined as

$$\Delta\rho = \rho[(H_2O)_n/Be] - \rho[(H_2O)_n] - \rho[Be], \quad (3)$$

while $n$ is the number of water molecules within a surface cell, $\rho[(H_2O)_n/Be]$ is the total electron charge density of the Be slab with waters, $\rho[Be]$ is the total charge density of the bare Be slab, and $\rho[(H_2O)_n]$ is the total charge density of the water molecules. In computing $\rho[Be]$ and $\rho[(H_2O)_n]$, the Be atoms and the water molecules are kept fixed at exactly the same positions as they are in physisorbed/chemisorbed systems.

For water monomer adsorption, it is easy to find out that there is an obvious charge accumulation in between the oxygen and the surface beryllium atoms (see Fig. 8(a) for details). Subsequently, in the dimer and the bilayer cases, the universal structures indicate that the water–surface interaction is localized principally in the lower water molecules, while the higher water molecules are almost unaffected by the substrate beryllium atoms, as shown in Figs. 8(b), 8(c), and 8(d). The electron density difference of these low-lying water molecules for the adsorbed dimer and bilayer is similar to that in the monomer water adsorption. The O–Be bond of the low-lying molecular in the water dimer adsorption is strongest due to the shortest $d_{O-Be}$. In the H-up water bilayer adsorption (Fig. 8(c)), the high-lying water molecule shows a quite weak hybridization with the metal substrate surface due to the very large distance between them. In addition, this observation also implies that the electron redistribution on the low-lying water molecule does not affect the electron density of the high-lying water molecules at all. In the H-down case, Fig. 8(d) shows that the H–Be bond of the high-lying molecule affects the electron redistribution considerably. Electronic charge transfer from the hydrogen to the surface beryllium atoms occurs. However, the H–Be bond does not appear because of the instability of the H-down bilayer adsorption on the Be(0001) surface.

# 4. Conclusion

The adsorptions of water monomers and water clusters on the Be(0001) surface have been investigated by using the DFT method and total-energy calculations. We have also presented a detailed picture of the electronic structure for the adsorptions by using surface work function analysis, the partial density of states, and the electron density difference. The aim of the present work is to shed light onto the general features of the water–simple metal adsorption systems. The essential results and the conclusions obtained in this work can be outlined as follows. Compared with transition and noble metals, we notice that the water adsorption on simple metal surfaces has a general rule for the water–metal interaction. i) The atop site adsorption is the most stable on all forms of water, including monomers, clusters, and bilayers. Each water molecule is laterally displaced from the precise atop position by no more than 0.15 Å in all studied models except for the trimer adsorption. ii) An expanded OH bond and a more open ∠HOH angle are found in the water monomer adsorption on the Be(0001) surface, and the structures of the adsorbed water monomers lie nearly parallel to the surface. iii) In the dimer and the bilayer adsorptions, the water–surface interaction is localized mainly in the low-lying water molecule. Among those adsorption configurations, the dimer is most stable with a peak adsorption energy of $\sim 437$ meV, while the H-down bilayer is extremely unstable, predicting that the H-down bilayer could not be adsorbed on the Be(0001) surface. The PDOS analyses reveal that the interactions between the water monomer and the Be(0001) surface are mainly contributed by electrons transferring from the $3a_1$-like water molecular orbital to s and $p_z$ electronic states of the beryllium atoms. In previous reports,[13,41] the $1b_1$-like orbital of the water molecule is the preferred adsorption site for transition and noble metals. Although the structural and the energetic predictions of the water–simple metal interaction have been discussed here without experimental references, it is expected to be useful for instructing further theoretical and experimental research on water adsorption on the Be(0001) surface.

# Acknowledgement

The last author (M. Q. Tan) would like to acknowledge the Program for Changjiang Scholars and Innovative Research Team in Universities under Grant No. IRT0754.

# References

[1] Morgenstern K and Nieminen J 2002 *Phys. Rev. Lett.* **88** 066102

[2] Morgenstern K and Rieder K H 2002 *J. Chem. Phys.* **116** 5746
[3] Mitsui T, Rose M K, Fomin E, Ogletree D F and Salmeron M 2002 *Science* **297** 1850
[4] Anderson S, Nyberg C and Tengstål C G 1984 *Chem. Phys. Lett.* **104** 305
[5] Nyberg C, Tengstål C G, Uvdal P and Anderson S 1986 *J. Electron Spectrosc. Relat. Phenom.* **38** 299
[6] Nyberg C and Tengstål C G 1984 *J. Chem. Phys.* **80** 3463
[7] Stuve E M, Jorgensen S W and Madix R J 1984 *Surf. Sci.* **146** 179
[8] Lloyd K G, Banse B A and Hemminger J C 1986 *Phys. Rev.* B **33** 2858
[9] Brosseau R, Ellis T H and Morin M 1990 *J. Vac. Sci. Technol. A* **8** 2454
[10] Thiel P A and Madey T E 1987 *Surf. Sci. Rep.* **7** 211
[11] Henderson M A 2002 *Surf. Sci. Rep.* **46** 5
[12] Michaelides A, Alavi A and King D A 2003 *J. Am. Chem. Soc.* **125** 2746
[13] Michaelides A, Ranea V A, de Andres P L and King D A 2003 *Phys. Rev. Lett.* **90** 216102
[14] Meng S, Wang E G and Gao S W 2004 *Phys. Rev.* B **69** 195404
[15] Ranea V A, Michaelides A, Ramírez R, Vergés J A, de Andres P L and King D A 2004 *Phys. Rev.* B **69** 205411
[16] Sebastiani D and Site L D 2005 *J. Chem. Theory Comput.* **1** 78
[17] Wang S W, Cao Y Z and Rikvold P A 2004 *Phys. Rev.* B **70** 205410
[18] Abramov E, Riehm M P, Thompson D A and Smelter W W 1990 *J. Nucl. Mater.* **175** 90
[19] Dietz K J and the JET Team 1990 *Plasma Phys. Contr. F.* **32** 837
[20] Kresse G and Furthmüller 1996 *J. Comput. Mater. Sci.* **6** 15
[21] Kresse G and Furthmüller 1996 *Phys. Rev.* B **54** 11169
[22] Kresse G and Joubert D 1999 *Phys. Rev.* B **59** 1758
[23] Blöchl P E 1994 *Phys. Rev.* B **50** 17953
[24] Perdew J P, Burke K and Ernzerhof M 1996 *Phys. Rev. Lett.* **77** 3865
[25] Methfessel M and Paxton A T 1989 *Phys. Rev.* B **40** 3616
[26] Monkhorst H J and Pack J D 1976 *Phys. Rev.* B **13** 5188
[27] Neugebauer J and Scheffler M 1992 *Phys. Rev.* B **46** 16067
[28] Bengtsson L 1999 *Phys. Rev.* B **59** 12301
[29] Hector L G, Herbst J F, Wolf W, Saxe P and Kresse G 2007 *Phys. Rev.* B **76** 014121
[30] Holzwarth N A W and Zeng Y 1995 *Phys. Rev.* B **51** 13653
[31] Davis H L, Hannon J B, Ray K B and Plummer E W 1992 *Phys. Rev. Lett.* **68** 2632
[32] Feibelman P J 1992 *Phys. Rev.* B **46** 2532
[33] Stumpf R and Feibelman P J 1995 *Phys. Rev.* B **51** 13748
[34] Antonelli A, Khanana S N and Jena P 1993 *Surf. Sci.* **289** L614
[35] Pohl K, Cho J H, Terakura K, Scheffler M and Plummer E W 1998 *Phys. Rev. Lett.* **80** 2853
[36] Sim F, Amant A S, Papai I and Salahub D R 1992 *J. Am. Chem. Soc.* **114** 4391
[37] Barnett R N and Landman U 1993 *Phys. Rev.* B **48** 2081
[38] Li J B, Zhu S L, Li Y and Wang F H 2007 *Phys. Rev.* B **76** 235433
[39] Doering D L and Madey T E 1982 *Surf. Sci.* **123** 305
[40] Michaelides A 2006 *Appl. Phys.* A **85** 415
[41] Carrasco J, Michaelides A and Scheffler M 2009 *J. Chem. Phys.* **130** 184707